Environmental Science: Atmospheres

ROYAL SOCIETY OF CHEMISTRY

PAPER

View Article Online
View Journal | View Issue

Cite this: *Environ. Sci.: Atmos.*, 2025, **5**, 1230

Wavelength-resolved quantum yields for phenolic carbonyls in acidic solution: molecular structure effects on brown carbon photochemistry

Dong Lee,† Ellery Moore,† Yiheng He, Tate Weltzin, Maria Gabbasova, Allen Zhu, Aidan Gee, Tom Rioux, Lindsey R. Madison* and Greg T. Drozd*

Light absorbing organic aerosol content, or brown carbon (BrC), affects climate through positive radiative forcing, may act as a photosensitizer in particle aging, and can directly play a role in the oxidative aging of organic aerosol. Wildfire emissions are a global source of BrC, and within wildfire emissions phenolic carbonyls (PhC) are some of the most photoreactive compounds emitted. Wildfire BrC components may have photochemical lifetimes of hours to days. Such a wide range in lifetimes makes detailed information on the products and mechanisms of BrC photochemistry critical in estimating effects of BrC on climate and aerosol chemistry. The aerosol chemical environment, particularly pH for aqueous aerosol, has strong effects on the reactivity of BrC, potentially altering absorption spectra and excited state reactivity. Various laboratory approximations of solar illumination have been used in studying the photochemistry of BrC compounds, making direct comparison between results difficult, and the relationship between chemical structure and reactivity of PhC is important for understanding and predicting BrC behavior and stability. In this work, aqueous photochemistry of six phenolic carbonyls (PhC) including coniferaldehyde (CA), 4-hydroxybenzaldehyde (4-HBA), 4-hydroxy-3,5-dimethylbenzaldehyde (DMBA), isovanillin (iVAN), vanillin (VAN), and syringaldehyde (SYR) was studied to elucidate relationships between structure, product formation, and photochemical mechanism. Using several narrow band UV-LEDs (295–400 nm), wavelength dependent quantum yields were calculated to allow direct comparison between photochemical experiments with laboratory irradiation sources and atmospheric actinic fluxes. Quantum yields were measured in acidic, air-saturated, aqueous solutions with pH = 2; conditions present in sulfate dominated aerosol or very acidic fog droplets. Computational results show that the electronic transitions leading to photochemical loss of PhC are nearly all $\pi \rightarrow \pi^*$, with conserved aspects of their electronic character. PhC photochemical quantum yields are concentration dependent, due to a direct reaction between triplet excited-state and ground-state PhC molecules, and maximum quantum yields of the range of structures studied span 0.05–2%. Wavelength dependent quantum yields are used to directly calculate the dependencies of photochemical loss on solar zenith angle (SZA).

Received 4th July 2025
Accepted 26th September 2025

DOI: 10.1039/d5ea00077g

rsc.li/esatmospheres

Environmental significance

Sunlight transforms the organic composition of atmospheric aerosol through complex photochemistry, with effects on aerosol absorption of solar radiation and its extent of oxidation. We studied the photochemistry of an important class of organic molecules that absorb UV radiation, phenolic carbonyls (PhC), and related their reactivity in acidic solution (pH = 2) to molecular structure. By using UV-LEDs as a light source, the wavelength specific quantum yields measured allow direct calculation of photochemical reaction for any condition (time/day/location). The arrangement of substituents affects ensuing radical reactions, with dramatic effects on the light absorption properties of the reaction products, and the nature of the molecular orbitals shows a clear trend across PhC structures. The importance of wavelength resolved measurements at conditions relevant to atmospheric aerosol is demonstrated.

1 Introduction

Atmospheric phenolic carbonyls (PhC) span a diverse range of chemical structures, including oxidation products of hydrocarbons, such as 4-hydroxybenzaldehyde, and oxidized derivatives of guaiacol and syringol such as vanillin and syringaldehyde, respectively. These compounds are emitted from biomass burning sources such as wildfires and domestic heating and are distinguished by the reactivity of the aldehyde and hydroxyl groups attached to the aromatic ring, along with their strong UV absorption *via* the conjugated aldehyde/

Department of Chemistry, Colby College, Waterville, Maine, USA. E-mail: gtdrozd@colby.edu
† These co-authors contributed equally.

aromatic system.[1,2] PhC are known to play a critical role in processes that lead to formation of both secondary organic aerosol (SOA) and light-absorbing organic compounds categorized as brown carbon (BrC).[3–13] Photochemistry initiated by BrC, including action as a photosensitizer, has been shown to be significant; it may even be competitive with radical and heterogeneous oxidation processes in aqueous aerosol, with significant impacts on formation and transformation of secondary organic aerosol (SOA).[7,14–18] The resulting SOA and BrC products produced by PhC lead to negative impacts on human health and global climate. Recent estimates suggest that, globally, BrC may have a warming potential that is approximately 20% that of black carbon.[19,20] While current studies address PhC impacts under a range of relatively specific conditions, links between PhC structure, photochemical mechanisms, and product formation have yet to be fully characterized.

The PhC studied are an important class of lignin-pyrolysis products from hardwood and softwood tree species as well as grasses and forest floor litter.[21–26] PhC are present in relatively low fractions of total gas/particle organic content from wildfires. The total contribution of substituted phenols has been estimated at less the 5% of wood burning, and PhC will be a smaller subset of substituted phenols, making them present at even lower levels, perhaps less than 1%.[1] This study focuses on the chemistry of aldehydic PhC, but ketones and organic acids will also be a significant fraction of PhC emissions.[23,24,26,27] While PhC are a small fraction of total wildfire emissions, they may comprise an important fraction of wildfire BrC. Siemens *et al.* show that in predominantly smoldering fires from a range of fuels single ring aromatic species with 2–3 oxygen atoms contribute roughly 20–30% of total BrC absorption for peat, sagebrush, and ponderosa pine, while this class of species may contribute up to 45% of total absorption from grass combustion emissions.[26] PhC are a photochemically active subset of this class, so PhC reactivity is important for a complete understanding of this ubiquitous fraction of biomass burning.[8] We have focused on PhC as these molecules absorb within the 300–400 nm range and their UV excitation can lead to increased oxidation in atmospheric water, as noted above, particularly highly concentrated aqueous aerosol.

Several factors combine to make extrapolating loss measurements to different solar zenith angle (SZA) challenging. The rate constant for photochemical loss, j, can be defined by:

$$j = \int \Phi_{\text{loss}}(\lambda) \cdot I_0(\lambda) \cdot \varepsilon(\lambda) \mathrm{d}\lambda \quad (1)$$

where Φ_{loss} is the quantum yield for loss, I_0 is the incident photon flux (photons per cm^2 per s), and ε the base-e molar absorptivity M^{-1} cm^{-1}. Eqn (1) applies to optically thin systems, requiring corrections for cases with less than 90% transmission of light. Quantum yields in higher energy, narrow wavelength excitation studies of PhC (*e.g.* 310 nm) show larger quantum yields than broadband studies (*e.g.* SZA of 0° or 45°), indicating wavelength dependent quantum yields for a wide range of atmospherically relevant substituted aromatics.[15,28] Conjugation between the aldehyde and the aromatic ring in PhC allows these molecules to absorb light within the photochemically active range of the solar spectrum (300–400 nm), with most absorption peaks centered near or below 340 nm, where both the intensity and wavelength dependence (shape) of the solar spectrum varies significantly with solar zenith angle (Fig. S1). The quantum yield for loss has been shown to have a strong wavelength dependence in this region.[29,30] Upon photon absorption, the PhC molecule becomes an excited singlet state, which rapidly undergoes intersystem crossing to form an excited triplet state. The excited triplet abstracts a hydrogen from ground state PhC through self-reaction or from another H atom donating molecule within the solvent, facilitating the formation of dimeric or oligomeric species as previously demonstrated.[29] This process has been shown to be dependent on the concentration and excitation wavelength, and it has been shown to be best modeled as a second order quantum yield for loss of vanillin.[29] In this work, we examined the aqueous photolysis of six PhC molecules commonly released during wildfire emissions: coniferaldehyde (CA), 4-hydroxybenzaldehyde (4-HBA), 4-hydroxy-3,5-dimethylbenzaldehyde (DMBA), isovanillin (iVAN), vanillin (VAN), and syringaldehyde (SYR). Quantum yields were determined as a function of excitation wavelength under acidic (pH = 2) conditions to determine structure–reactivity relationships.

2 Methods

2.1 Materials

All reagents (coniferaldehyde: 98%, 4-hydroxybenzaldehyde: 95%, 4-hydroxy-3,5-dimethylbenzaldehyde: 95%, syringaldehyde: 98%, isovanillin: 95%, vanillin: 99%) were purchased from Sigma-Aldrich and used without further purification. Chemical structures are shown in Fig. S2. Stock solutions (3–5 mM) were prepared in acetonitrile (Sigma-Aldrich, >99.9%); photolysis solutions were prepared by diluting stock solutions with 18 MΩ deionized water; pH was adjusted using HCl (1 N, Titripur). HPLC solvents were prepared with 18 MΩ deionized water, acetonitrile (Sigma-Aldrich, HPLC-Plus, >99.9%) and formic acid (Sigma-Aldrich, >95%).

2.2 Illumination source characterization

6 UV-LEDs (Violumas) with nominal wavelengths of 300, 318, 325, 340, 375, and 385 nm were used to illuminate aqueous phenolic carbonyl solutions. The LEDs were connected to a Tekpower TP1803D variable DC power supply (0.1–0.8 A). The spectral profiles were taken at similar intensities as shown in Fig. 1. The photon flux was determined using 2-nitrobenzaldehyde (2-NBA) as an actinometer, which has a known constant quantum yield (0.43) between 300–400 nm.[31,32] The conversion of NBA to 2-nitrosobenzoic acid upon illumination was monitored using HPLC analysis (Agilent 1100 series, Agilent Technologies GmbH, Germany), observing 6–7 timepoints over a period of 2–3 lifetimes. Actinometry was monitored daily using an Agilent Cary 60 UV-vis spectrometer to check for consistency in the time for approximately 50% loss of NBA, full actinometry was performed weekly or if UV measurements

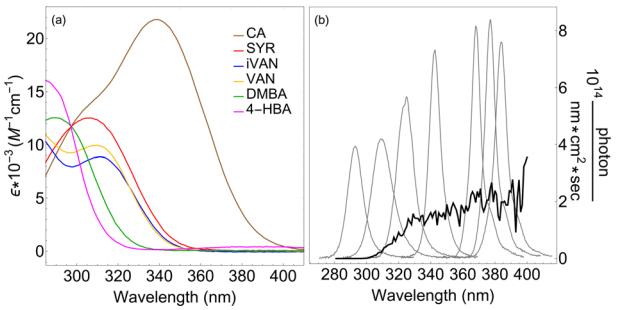

Fig. 1 (a) The molar absorptivity (base-10, aqueous, pH = 2) of PhC molecules in the most photochemically active range of the solar spectrum (300–400 nm). (b) The LED illumination source profiles (gray) for nominal wavelengths of 300, 318, 325, 340, 375, and 385 nm with solar irradiance at 45° SZA (black).

showed more than 10% variance. Typical peak irradiance for LED varied in the range 1–40 × 10^{14} photons per nm per cm^2 per s.

2.3 UV measurements

An Agilent Cary 60 UV-vis spectrometer was used to measure absorbance spectra for all molecules to calculate quantum yields. These spectra are shown in Fig. 1, with chemical structures shown in Fig. S2. Absorbance measurements were taken over the range of 200–800 nm.

2.4 Photolysis experiments

1.0 mL of PhC solution was added to a quartz vial (Technical Glass Products, 15 mm dia.) with UV-LED illumination from below, giving a pathlength of 0.88 cm. Solution absorbance was maintained below 0.2 in all solutions to minimize internal screening, which was corrected as in previous work.[29] For shorter experiments fresh solution was used for each time point, and for longer experiments aliquots were removed, never reducing total solution volume by more than 10%. Vials were tightly sealed with a Teflon lined screw cap to prevent evaporation. Laboratory temperature was 23 ± 3 °C. All samples were prepared with pH = 2, as atmospheric particle pH is generally observed to be between 0 and 4, with an approximate range recently considered to span −1 to 5.[19,33,34] Cloud or fog droplets generally have higher pH, approximately 2–7.[35] While pH = 2 is representative to both aerosols and very acidic cloud/fog droplets, other solution properties, such as ionic strength, are present at levels more dilute, which are more relevant to cloud droplets.

2.5 HPLC analysis

The HPLC system has both ToF-MS and a diode array (DAD) detectors. The DAD was equipped with a 500 nL flow cell, 10 mm pathlength, using a reference wavelength of 700 nm. The electrospray ion source of the MS was operated using the following setup: nebulizer pressure 2400 mbar, drying gas flow 8 L min^{-1}, dry gas temperature 325 °C, and spray voltage 3500 V. Quantification of each phenolic carbonyl was determined using calibration from the UV chromatograms of known standards. Eluents consisted of ultrapure water (eluent A) and acetonitrile (eluent B) both with 0.1% formic acid. Actinometry measurements were taken with a flow rate of 0.75 mL min^{-1} using a mobile phase set to 35% B for 1.90 minutes and analyzed at 227 nm with a reference of 700 nm. PhC measurements excluding 4-hydroxy-3,5-dimethylbenzaldehyde were taken using a 0.500 mL min^{-1} flow rate with the following method: starting with 15% B, isocratic for 5 minutes, followed by an increase to 100% B over 0.1 minutes, a hold at 100% B for 0.5 minutes, a decrease back to 15% B over 0.1 minutes, and a hold at 15% B for 0.3 minutes. 4-Hydroxy-3,5-dimethylbenzaldehyde measurement was taken using a 0.500 mL min^{-1} flow rate with the following method: starting with 40% B, isocratic for 2.4 minutes, followed by an increase to 100% B over 0.1 minutes, a hold at 100% B for 0.5 minutes, a decrease to 40% B in 0.1 minutes followed by a hold at 40% B for 0.9 minutes.

2.6 Kinetic analysis

The quantum yield for photochemical loss, Φ_{loss}, is defined as

$$\Phi_{loss} = \frac{R_{loss}(t=0)}{R_{abs}(t=0)} \quad (2)$$

where $R_{loss}(t=0)$ is the initial rate of loss of PhC and $R_{abs}(t=0)$ is the initial rate of photon absorption over the entire range of illumination wavelengths. Molar absorptivity measurements (Fig. 1) are used to determine the initial absorption rate. By fitting a curve to the observed time-dependent concentration data, the initial rate of loss can be estimated using an appropriate kinetic rate law. First order kinetics have generally been applied to model the loss of PhC molecules, but as we have previously observed for VAN, PhC may exhibit mixed-order kinetics, as indicated by the concentration dependence of Φ_{loss} on the concentration of ground state PhC.[28,29] The quantum yield for loss of PhC is written as

$$\Phi_{loss} = \Phi_{ISC} \cdot \frac{k_{SR}[PhC]}{k_1 + k_{SR}[PhC]} + \Phi_1 \quad (3)$$

where Φ_{ISC} is the quantum yield for intersystem crossing, k_{SR} describes the self-reaction between ^{3}PhC* (typically the protonated form of ^{3}PhC* at pH = 2) and ground state PhC. Φ_1 describes any loss not caused by self-reaction (*e.g.* Norrish-type reaction). k_1 describes the sum of triplet deactivation processes, which can include quenching by oxygen and/or solvent. For a polychromatic light source, such as solar radiation, eqn (1) and (3) can be combined to determine the rate of loss of PhC.

$$\frac{d[PhC]}{dt} = -[PhC] \cdot \int_\lambda \left(\frac{\Phi_{ISC} k_{SR,\lambda}[PhC]}{k_1 + k_{SR,\lambda}[PhC]} + \Phi_1 \right) I_0(\lambda)\varepsilon(\lambda) d\lambda \quad (4)$$

This expression simplifies to purely second order in [PhC] when k_1 is much faster than self-reaction and loss *via* ^{3}PhC* is greater than direct photolytic loss.

There is significant support for this mechanistic model concerning both triplet state involvement and reaction between ^{3}PhC* and ground state PhC. The involvement of PhC triplet states is supported by triplet quenching and resulting decreases

in Φ_{loss} or ^{3}PhC* lifetime in the presence of dissolved oxygen, as well as transient UV spectra consistent with triplet state formation.[7,29,36] Several kinetic parameters have been shown to be dependent on the concentration of PhC, including the lifetime of ^{3}PhC*, the rate constant for loss (in acidic conditions), and Φ_{loss}.[7,28,29] Previous work from this group showed a linear relationship between Φ_{loss} and [VAN] for wavelengths spanning 295–340 nm.[29] In the current study, all six PhC studied had a clear increase in Φ_{loss} with increasing PhC concentration, with an average ratio for $\frac{\Phi_{loss}(20\ \mu M)}{\Phi_{loss}(10\ \mu M)}$ of 1.85. These are clear indications of reaction between excited state and ground state PhC.

2.7 Computational methods

UV-vis absorption spectra of the reactants were computationally predicted using vertical excitations from the ground state *via* TD-DFT with Gaussian 16.[37] All molecules were minimized on the ground electronic state, S_0, using the hybrid functional B3LYP,[38–41] the 6-311+G(2d,p) basis set,[42,43] and an implicit PCM solvent to replicate the effect of an aqueous environment (ε = 78.3553).[44] Electronic excitations from the minimum energy structure were performed at the same level of theory, B3LYP/6-311+G(2d,p), using nonequilibrium aqueous solvent conditions (ε_{inf} = 1.7778). Natural Transition Orbitals (NTO),[45] visualized with GaussView,[46] were used to characterize the hole and the electron character of the excited states with the highest oscillator strengths. Natural Transition Orbitals are representations of the electron density rearrangement due to an excitation and are found from a singular value decomposition of the one-particle transition density matrix. NTOs depict the originating orbital (hole) and the destination orbital (electron).

3 Results and discussion

3.1 PhC absorption spectra and characterization of electronic transitions

All PhC molecules have one or two absorption band centers in the 270–400 nm range. Our calculated excitation energies from optimized ground state structures show good agreement with experiment (Table 1), with PCM solvent improving the agreement between theory and experiment (Tables S1 and S2). Calculated excited state transitions are shown in Fig. 2 and direct comparisons with experimental spectra are in Fig. S3. Recent studies contain ambiguities as to whether these transitions correspond to n → π* or π → π* transitions.[47,48] Our computational analysis reveals that these correspond to π → π* transitions; the character of these transitions is defined largely by changes in occupation of π type orbitals on the aromatic ring with amplitude contributed from the carbonyl oxygen contributing in a π* and out-of-phase manner. The excited states are labeled based on their energetic ordering for each molecule. The S_1 state for VAN, iVAN, SYR, 4-HBA, and DMBA is indeed an n → π* transition, however the oscillator strength is very low (<0.001) indicating the forbidden nature of the transition. CA has the strongest absorption of all six molecules, and its spectrum extends to much longer wavelengths, out to 370 nm. The red shift of the CA transitions and their stronger absorption can be interpreted following principles of particle in a box; the hole and electron NTOs of both transitions have greater delocalization on the propenal group, stabilizing

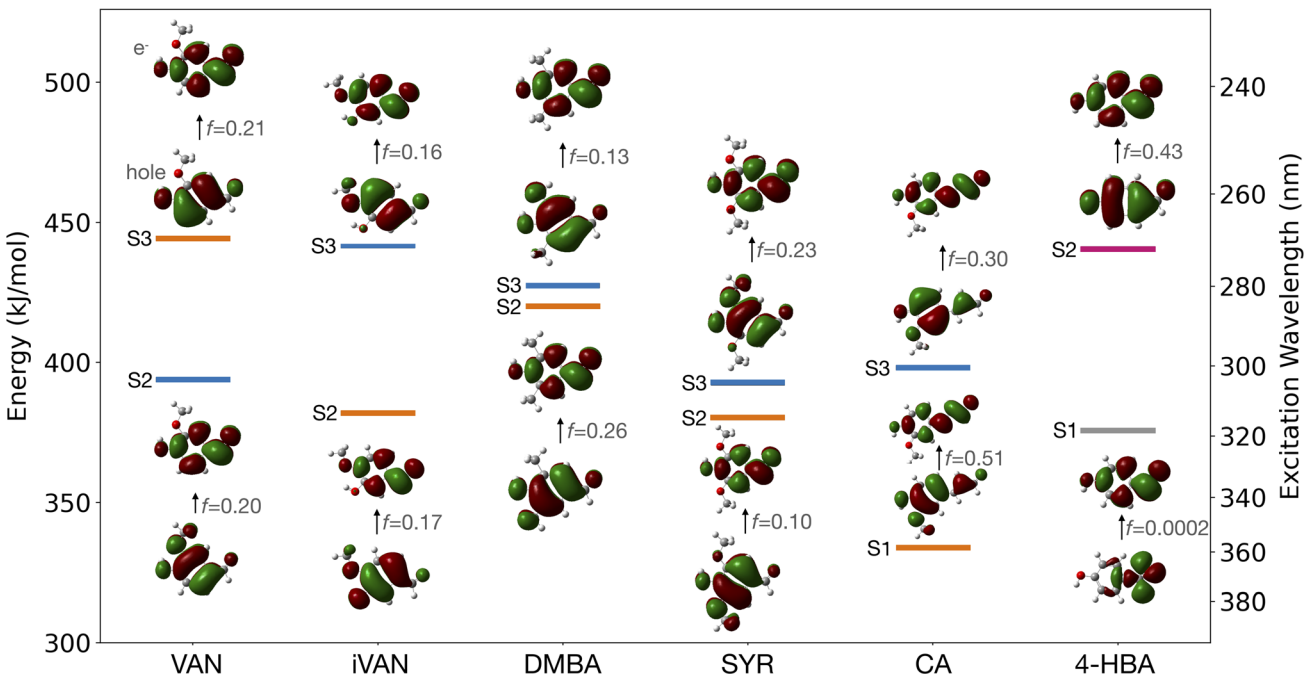

Fig. 2 Excited states corresponding to excitations from S_0 between λ = 250 and λ = 400 nm with significant oscillator strengths. The Natural Transition Orbitals (NTOs) depict the originating orbital (hole), and the destination orbital (electron) for each transition from S_0 to the respective states.

Table 1 Centers of absorption bands (nm) of PhC between 260–500 nm representing the π → π* transitions. Asterisks indicate an n → π* transition. Computed oscillator strengths are included in parentheses following the TD-DFT transition wavelength

PhC	Absorption band 1	TD-DFT	Absorption band 2	TD-DFT
Vanillin	279	269 (0.21)	310	304 (0.20)
iVAN	279	272 (0.16)	311	313 (0.17)
DMBA	290	279 (0.13)		
		285 (0.26)		
SYR	307	305 (0.23)		
		315 (0.10)		
CA	306	300 (0.30)	339	354 (0.51)
HBA	284	272 (0.43)	392*	318* (0.0002)

the energy of the transition and contributing to larger transition dipole moments. Unlike all other PhC studied, the S_1 state of CA is identified as π → π*, and for CA a dark n → π* transition is predicted at 340 nm. 4-HBA is the only molecule to exhibit a weak, yet observable n → π* transition, centered at 392 nm. As expected, this n → π* transition is about 40× weaker than the 4-HBA π → π* transition at 284 nm (Table 1).

The calculated electronic transitions for the PhC studied show the effects of molecular symmetry and substitution on their absorption spectra. While a single, strong π → π* transition appears for SYR and DMBA, in fact these peaks are created by two nearly degenerate transitions. The near symmetry of DMBA and SYR manifests in near degeneracy of the S_2 and S_3 states, with symmetry broken by the hydroxyl and carbonyl orientation toward either the methyl or methoxy groups. For the rest of the PhC, energetically well separated π → π* transitions appear as two separate and narrower transitions. The orientations of the nodes of the hole and electron orbitals of the NTOs reveal variation in the nature of the transitions across the molecules. Fig. 2 includes a color scheme that distinguishes the states by the orientation of the nodes of the hole orbitals relative to the carbonyl group. Excluding 4-HBA, the lowest energy π → π* transitions have hole NTOs that point diagonally towards (blue) or away (orange) from the aldehyde group. Only VAN has its lowest NTO with the former orientation. The bright transition of 4-HBA corresponds to a unique π → π* transition, with a vertical orientation of the nodes on the ring orbital. VAN and iVAN have nearly identical transition energies for excitations to the first two bright states, despite the reversed ordering of the orientation of their hole NTO. This suggests an impact of the locations of the hydroxyl and/or methoxy group on the hole character of the NTO. We also see that the lower energy transition at 310 nm is conserved across a series of PhC structures, yet the higher energy π → π* transition shifts from 280 nm for VAN and iVAN to 305 nm for SYR, which has an additional methoxy substituent.

3.2 Mechanism, product formation, and product spectra

Mechanistically, VAN serves as a prototypical PhC from wildfire emissions; it has been observed in relatively high proportion in biomass burning emissions and has been investigated more than other PhC.[1,7,28,36,47,49–53] Guided by previous work on VAN, a proposed mechanism for PhC photochemistry is shown in Fig. 3, along with structures of key radical intermediates.[29,36] After photoexcitation in either aqueous or polar aprotic solutions, an excited state PhC reacts with a ground state PhC to undergo hydrogen abstraction, leading to a second order loss pathway.[7,15,28] Our previous study of vanillin also suggests the potential for direct photodissociation, a first order loss process, to be important at lower concentrations.[29] Both pathways may lead to the formation of radical species that form stable dimer products through radical coupling.[7,29,36] Dimers were identified *via* ToF-MS at 2 amu less than twice the molecular mass of the respective PhC monomer. We only definitively observed dimer formation for VAN, iVAN, and CA. Photoexcitation of SYR did not result in dimer production, in agreement with a previous study;[48] additional peaks in the UV chromatograms of SYR products indicate an alternative mechanism for loss of PhC, likely involving other processes such as photofragmentation.[12] For SYR and DMBA, dimerization may be prevented because both *ortho* positions as well as the *para* position relative to the hydroxyl group are occupied. New-bond formation at these positions is favored by radical stability and the ability to regain aromaticity after H-atom abstraction by O_2 (blue step in Fig. 3). This relationship between structure and reactivity also suggests the importance of reaction between $PhC^{\bullet}_{(-H)}$ radical and a closed-shell PhC. 4-HBA, with no electron donating substituents, may not be stable enough to have a lifetime permitting reaction leading to dimer products.

Our inferences about molecular structure and dimer formation are further supported by the UV spectra of the products, shown in Fig. 4. The only structure with an abstractable H-atom *para* to the phenolic group is iVAN, and the total spectrum of its products is remarkably different from the UV spectra of the other PhC studied. First, the π → π* transition near 280 nm is nearly unchanged in the products, with only a minor redshift. This is shown clearly by the overlap of the black and red lines in the lower left panel of Fig. 4. Second, the iVAN products have a distinct peak at 350 nm which is most likely attributed to a dimer formed *via* H-atom abstraction and new bond formation at the *para* position relative to the initial phenolic group. Photoproducts from VAN, with only an open *ortho* position relative to the phenol, show only slight enhancement of long-wavelength absorption. Notably, Smith *et al.* observed much stronger long-wavelength absorption for products in experiments with much higher VAN concentration (100 μM), less acidic solution (pH = 5), and broadband illumination.[28] Future investigation on the variation of the product distribution with reaction conditions is needed. CA, despite clear evidence of dimer formation from MS-ToF spectra, has minimal enhancement of absorption at long wavelengths. This can tentatively be attributed to the importance of the unique resonance structure of its $PhC^{\bullet}_{(-H)}$ radical (Fig. 3.) that can lead to formation of dimers with reduced conjugation, which would not enhance long-wavelength absorption. Reaction mixtures from 4-HBA and DMBA do not show the presence of dimers in the MS-ToF results and no enhancement of long-wavelength absorption.

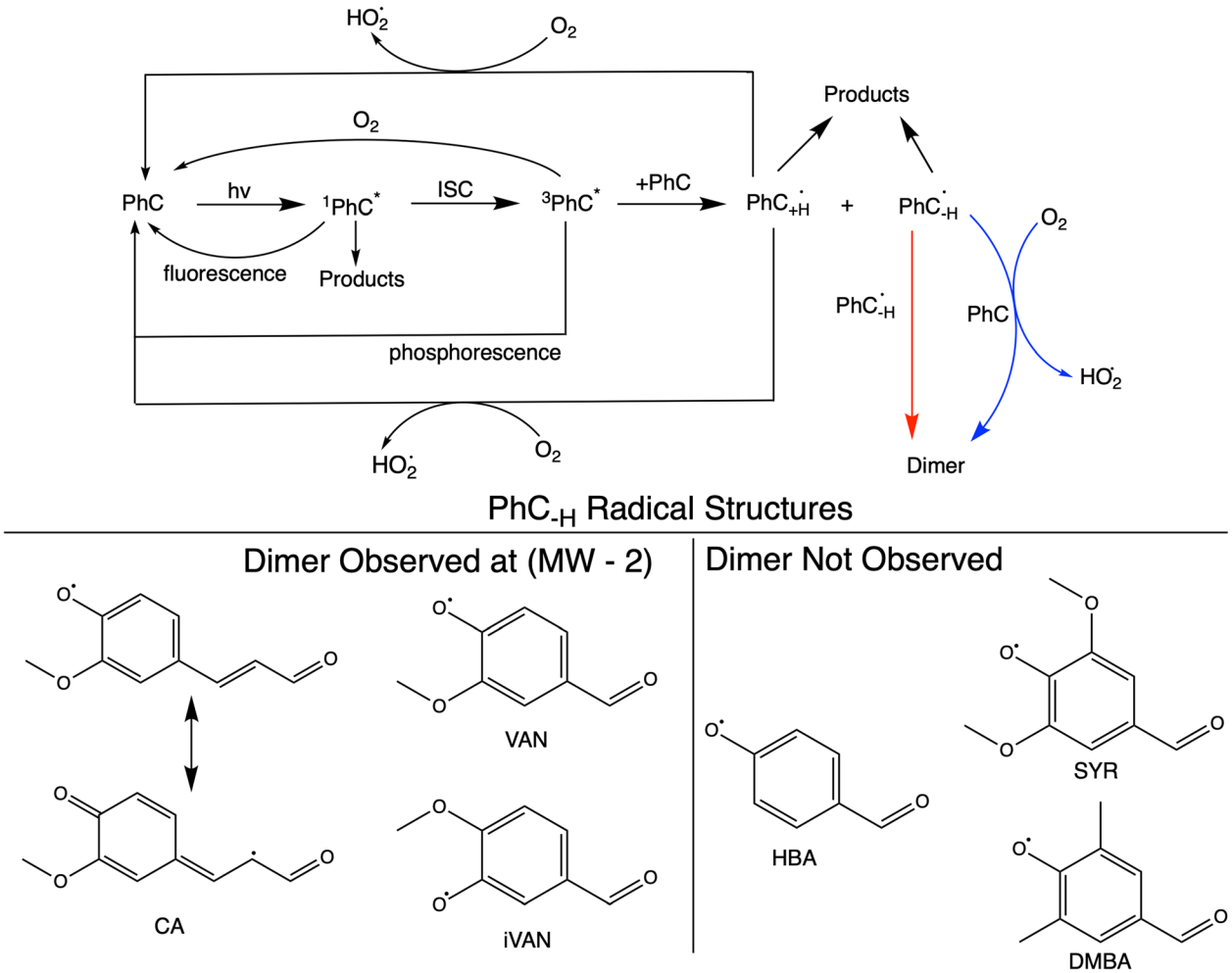

Fig. 3 Mechanism for photochemical loss of PhC. Radical propagation through excited triplet and ground PhC state reactions produce hydrogen abstracted radical structures. CA produces a unique radical structure, compared to the other PhC, due to additional conjugation.

While enhancement of longer wavelength absorption occurs for photochemical aging of PhC, they present just one of many compound classes in wildfire aerosol, particularly when considering aging effects. Aside from aromatic carbonyls, nitroaromatic compounds are an important class of primary combustion emissions, and they may often be more than 50% of BrC, depending on fuel type.[5,23,26,54] Nighttime (dark) aging BrC from combustion of wildfire fuel types has shown significant nitration of aromatic compounds leading to increased absorption well beyond 400 nm.[55] Reactions of aromatic compounds emitted from wildfires with iron has shown increased absorption well into the visible range.[56–58] Polycyclic aromatic hydrocarbons (PAH) likely contribute less than 10–15% of primary emissions, but their absorption may increase with nitration as well.[26] PhC thus contribute a fraction of total BrC absorption yet present an important class of photoreactive BrC.

3.3 PhC quantum yields

3.3.1 Structure effects on maximum Φ_{loss} values. The Φ_{loss} for the PhC structures in this work have maximum values of 0.05–2% within the photochemically active range of 300–400 nm in acidic (pH = 2) air-saturated, aqueous solutions. The trends in maximum Φ_{loss} are correlated with both photophysical PhC properties and the structure and stability of the radicals formed after hydrogen atom abstraction by their respective triplet states. Focusing on the unconjugated, non-methyl substituted PhC, maximum quantum yields decrease in the order: SYR (2%) > iVAN (1.5%) > VAN (1%) > 4-HBA (0.5%). The greater substitution for SYR facilitates hydrogen abstraction leading to greater loss,[59] to be discussed further in Section 3.5. In comparing the isomers of VAN, radical reactivity likely leads to greater Φ_{loss} for iVAN. After hydrogen abstraction, iVAN has an extra, stable resonance structure with the unpaired electron at the position *para* to the hydroxyl group. VAN has its hydroxyl group *para* to the aldehyde, preventing formation of this stable structure. 4-HBA is the least substituted species, which may cause slow hydrogen atom abstraction and lead to the lowest maximum Φ_{loss}. DMBA has a maximum Φ_{loss} (1.3%) that is slightly greater than VAN, potentially due to the influence of steric hindrance on the radical and increased lifetime for reaction prior to oxygen quenching. CA has a maximum Φ_{loss} (1.1%) which is slightly above its closest analogue, VAN, likely

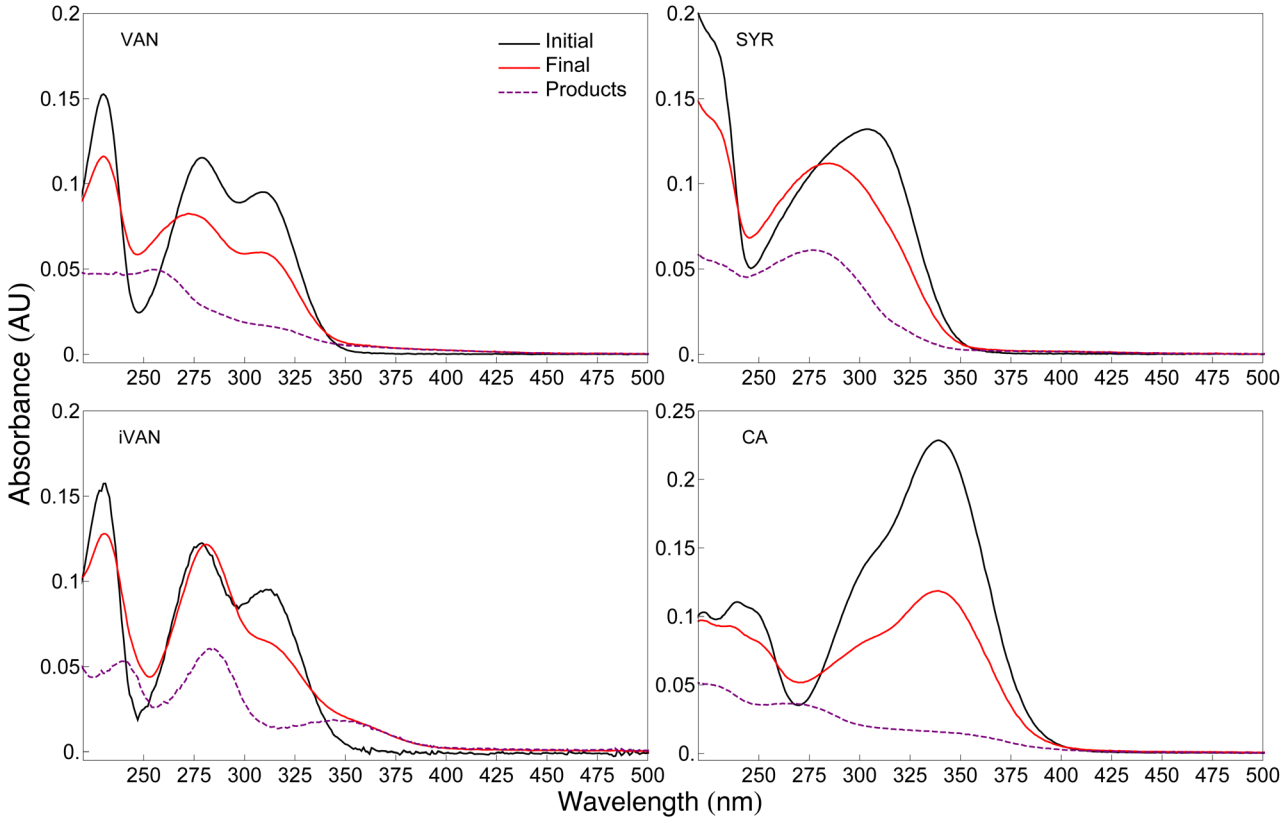

Fig. 4 UV-vis absorbance spectra for reaction mixtures with VAN, iVAN, CA, and SYR. Initial and final spectra of reaction mixtures are shown black and red, respectively. The spectra of the products are determined by subtracting any residual reactant (≈50% remaining), with the fraction of reactant remaining determined by HPLC analysis. The final spectra show that in general the products are more weakly absorbing than the reactants in the 220 nm to 325 nm range. The products for iVAN show significantly enhanced absorption above 340 nm, while products from its isomer VAN show much less enhancement. All other PhC studied show no enhancement in absorption at long wavelengths.

due to increased reactivity and stability from extra radical positions afforded by conjugation. The importance of radical reactivity effects on Φ_{loss} is further evident in comparing recent computational results for intersystem crossing rate constants and observed quantum yields.[30] The trend in peak k_{ISC} is Syr > VAN > iVAN > 4-HBA, largely following extent of substitution; the trend in Φ_{loss} is the same except for iVAN > VAN. The greater k_{ISC} for VAN compared to iVAN would be expected to translate to a larger maximum Φ_{loss}. We observe the opposite, further suggesting the importance of radical reactivity in determining Φ_{loss}.

While this study focuses on chemical structure effects on PhC photochemisty, maximum quantum yield values will also vary with chemical environment, particularly pH and ionic strength. Smith and Anastasio showed that ^{3}PhC* will be fully protonated at pH = 2, and the protonated form has Φ_{loss} that is approximately half that of the non-pronated form. The apparent pK_a of protonated excited state PhCs is approximately 4, so the value of Φ_{loss} will approximately double moving from pH = 2 to pH = 5.[28] While relatively low concentrations (<15 mM) of SO_4^{2-} and Cl^- ions were shown to have negligible effects on PhC photochemical loss, previous work on VAN from our group shows that much higher ionic strength can affect Φ_{loss}, with Φ_{loss} approximately doubling as ionic strength, adjusted by NaCl, increases from below 0.1 M to 3 M.[29]

3.4 Wavelength dependent Φ_{loss} for PhC

PhC separate into two groups when considering the wavelength dependence for Φ_{loss} in the 300–400 nm range: monotonic decay to long wavelengths or the presence of a local maximum at an intermediate wavelength. The first group includes VAN, iVAN, DMBA and SYR. For this group, Φ_{loss} is highest at the shortest wavelength, 300 nm, with exponential decay to approximately zero at λ < 370 nm with a Gaussian profile. This data is collectively shown in Fig. 5, and individually with uncertainties, in Fig. S4. For this group of molecules, photochemical loss is expected to be insignificant in the atmosphere at 370 nm compared to shorter wavelengths. 4-HBA would likely present a similar trend, but its narrower absorption spectrum prevents significant loss above 325 nm. Within our experimental uncertainty, Φ_{loss} is relatively constant for 4-HBA in the 300–325 nm range, indicating excited state processes leading to loss are relatively insensitive to excitation energy. Oscillator strength appears to be the main factor causing the observed wavelength threshold in Φ_{loss} for 4-HBA.

Φ_{loss} for CA exhibits a different trend than the other PhC molecules studied. In Fig. 5, CA shows an increase in Φ_{loss} from 300 nm to a peak at 325 nm, and then a rapid decline until reaching effectively zero at 380 nm.

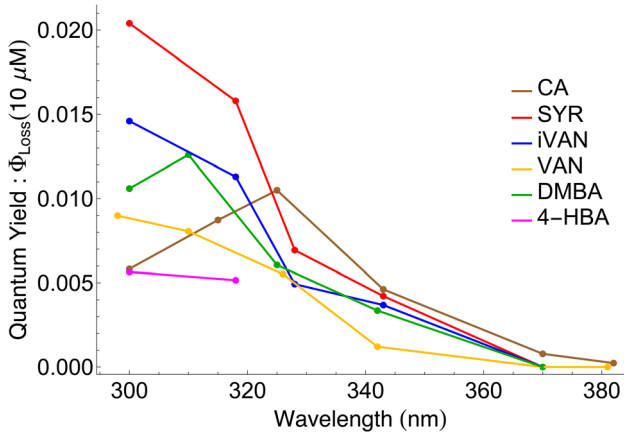

Fig. 5 Quantum yield for aqueous (pH = 2) loss measurements at 10 μM concentration for all PhC molecules studied.

Theoretical work based on time dependent density functional calculations (TDDFT-CAM-B3LYP/6-31G**) including spin orbit coupling suggests that this unique wavelength dependence may come from a wavelength dependent intersystem crossing rate constant.[30] The increased π-electron conjugation in CA reduces the adiabatic energy gap between S_1 and the destination triplet state. The adiabatic gap in CA was calculated to be significantly smaller (1630 cm^{-1}) than for the other PhC molecules investigated (5, 100 cm^{-1}), displayed in Valiev *et al.*[30] Essentially this smaller energy gap for CA leads to a complex, energy dependent Franck–Condon overlap, with a greater effective density of states at lower excitation energies, enhancing intersystem crossing.[30] Within our experimental uncertainty DMBA does not appear to group with CA in terms of the functional form for Φ_{loss} (Fig. S4), but it is possible that measurements at wavelengths below 300 nm could reveal DMBA to have a similar profile for Φ_{loss} as CA, just shifted to shorter wavelengths.

3.5 Solar zenith angle dependence of atmospheric rate constants and lifetimes

3.5.1 Solar zenith angle dependence of photochemical rate constant. Predicting loss of PhC in the atmosphere requires determining the effect of SZA on the rate constant for photochemical loss. As shown in eqn (4), this requires integrating the product of fits to Φ_{loss} (Fig. S4), light intensity (I_0), and molar absorptivity (ε), all of which are strong functions of wavelength. Concentration dependent, pseudo-first order rate constants at [PhC] = 10 μM, j_{eff} (10 μM; SZA), were calculated to determine the effects of PhC structure on atmospheric lifetime. These results are shown in Fig. 6a.

The SZA dependence for atmospheric loss is described by the maximum value at 0° SZA and the steepness of the fall-off towards 90° SZA. CA has the greatest j_{eff} (10 μM; 0°) of all PhC studied due to the greater overlap of its absorption spectrum and quantum yield with the solar spectrum. This is a direct result of the conjugation of the aldehyde and the aromatic ring through a C–C double bond. The peak value for Φ_{loss} of CA is nearly half that of SYR (Fig. 5), emphasizing the importance of the overlap of both Φ_{loss} (λ) and ε (λ) with I_0 (λ) in determining j_{eff} (SZA). Dictated by the decreasing total solar flux with greater SZA, all PhC have similar trends for j_{eff} (SZA), with the main difference across PhC structures being the steepness of decay with increasing SZA. Fig. 6a and its inset show that a smaller j_{eff} (0°) will correlate with a steeper decline with increasing SZA, thus 4-HBA (magenta) has the sharpest SZA dependence and CA (brown) has the most gradual decline with increasing SZA. This is explained in part by comparing ε (λ) across PhC. With increasing SZA, short wavelength light is reduced more strongly than longer wavelength light (Fig. S1), so molecules that do not efficiently absorb at longer wavelengths are more sensitive to SZA (*e.g.* 4-HBA) than those with broader spectra extending to long wavelengths (*e.g.* CA). As mentioned above, trends in Φ_{loss} (λ) may not follow ε (λ), further reinforcing the importance of the overlap of both Φ_{loss} (λ) and ε (λ) with I_0 (λ) in determining j_{eff} (SZA).

j_{eff} (10 μM; 60°) values for CA, SYR, and VAN can be compared to those estimated in Smith *et al.*[28] Rate constants for VAN and SYR are approximately 30% higher than the values reported in Smith *et al.*, and our bottom-up calculation for CA gives a j_{eff} (60°) that is 2.2× higher than the extrapolated value reported in Smith *et al.* In practical terms, both estimates for CA indicate very fast loss and correspondingly short lifetime on the order of minutes. Our calculated value should be a more direct estimation of loss with the solar radiation, as we can directly calculate j_{eff}. Without directly using solar radiation, broadband source measurements require a conversion to solar radiation, which may in part account for differences in estimated rates of loss. In addition, calibration differences, and, to a lesser extent,

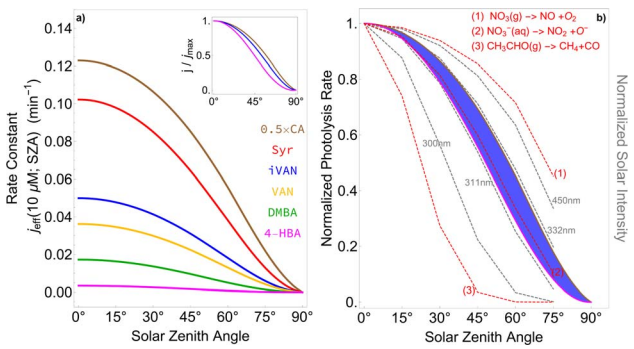

Fig. 6 (a) Pseudo first-order rate constant as a function of solar zenith angle (SZA) for each PhC at 10 μM concentration, j_{eff} (10 μM; SZA). For all molecules, the maximum rate of loss occurs at 0° SZA (noon equinox at Equator) then gradually declines until 30° SZA (noon equinox at 30° N latitude). j_{eff} then decreases rapidly after 30° SZA until reaching zero at 90° SZA (local sunset). Values for CA were multiplied by 0.5 for clarity of presentation. The inset shows the shape of $\frac{j}{j_{max}}$ as a function of SZA for CA, iVAN and 4-HBA. (b) Range of SZA dependence for all PhC studied, with j_{eff} normalized to j_{eff} (0°) (blue area), normalized intensity of solar radiation (gray, dashed line), and photolysis of $NO_3(g)$, $NO_3^-(aq)$, and $CH_3CHO(g)$ (red, dashed lines). Data for solar spectra and reaction rates were obtained from the NCAR TUV Model.

kinetic fitting (first order *vs.* second order), may also contribute to these discrepancies.

Fig. 6b juxtaposes the SZA dependence of PhC with the SZA dependence of three common atmospheric reactions and several wavelengths of sunlight. The blue shaded region shows the range of SZA dependence for aqueous PhC photochemical loss. In the 0°–75° SZA range, gas phase nitrate radical photolysis has a much weaker dependence on SZA than PhC, while gas phase photolysis of acetaldehyde has a much stronger SZA dependence. The aqueous photolysis of nitrate ion has a similar SZA dependence to photochemical PhC loss. The range of PhC studied has photochemical loss rates that span the same SZA dependence as 311–332 nm solar radiation. The SZA dependence of specified wavelengths of solar radiation provides a standard metric for comparing the SZA dependence of atmospheric photochemical processes. For example, aqueous nitrate ion has the same SZA dependence as 315 nm solar radiation.

A more quantitative comparison of the SZA dependence of j_{eff} for PhC is enabled with the analytical form in eqn (5).

$$j_{eff} = j_{max}([PhC]) - \frac{\beta([PhC])}{1 + e^{-\frac{SZA - SZA_C}{\omega}}} \quad (0^\circ < SZA < 90^\circ) \qquad (5)$$

In this equation, the parameters j_{max} and β scale the magnitude of j_{eff}, and both are required to ensure accuracy better than 5% due to potential asymmetry in the SZA dependence of molecules whose Φ (λ) and ε (λ) extend to longer wavelengths (*e.g.* CA). Both j_{max} and β will depend on concentration due to self reaction of PhC, while the shape parameters SZA_C and ω are much less sensitive to concentration. SZA_C describes the center of the fall-off curve, where $j_{eff} = 0.5\, j_{max}$, and ω defines the steepness of the approach to SZA_C. Together SZA_C and ω define the symmetry of the function within the defined input range of 0–90°. The values for the shape parameters follow a clear trend (Table 2), with more complex, longer wavelength absorbing species having larger SZA_C and ω values, as their profiles in Fig. 6 are shifted to larger SZA. All the fits are accurate to within 2% of the calculated j_{eff} and match the functional form as well (*i.e.* good derivative matching), as shown in Fig. S5.

While the concentration dependencies of j_{max} and β for PhC complicate broad application of eqn (5), it is important to note that other aerosol or droplet conditions will likely play a large role in predicting the rate of photochemical loss of PhC and other photochemically active species, particularly triplet species. In an actual aerosol particle or droplet, concentrations of other organic components will often be significant (*e.g.* >1 M), and many will be highly oxidized.[60,61] Oxidized organic compounds will likely function as H-atom donors, and their high concentration may make them competitive H-atom donors. This gives the organic matrix the potential to significantly alter aerosol/droplet photochemistry, making clear the need to examine aerosol photochemistry in more complex, yet specified, organic matrices.[62–64]

3.5.2 Solar zenith angle dependence of atmospheric lifetimes. Atmospheric lifetime is an essential quantity in assessing warming effects of BrC compounds in aerosol. It should be noted that the lifetimes calculated in this work are pseudo first order; if purely second order kinetics were present in the complex environment of an atmospheric aerosol, PhC would persist at low levels for significantly longer periods. Given the importance of H-atom transfer in the loss of PhC and the extreme abundance of H-atom donors (*i.e.* the sum of hydroxylated organic compounds) in atmospheric aerosol, it is likely that a pseudo first order approximation is applicable in atmospheric aerosol, but estimating the effect of abundant H-atom donors in aqueous atmospheric phases remains an important focus for future research. Fig. 7 demonstrates the sensitivity of atmospheric lifetime to SZA for all PhC studied, comparing lifetimes at 0° and 60° SZA. The range of lifetimes is quite large, <10 minutes to >1000 minutes, when including DMBA and 4-HBA. Within the methoxy-substituted PhC, the range of lifetimes is much narrower, <10 minutes to 80 minutes, and this class of PhC is much more prevalent in biomass burning emissions.[1] The ratio between the lifetime at 0° SZA and 60° SZA (Fig. 6 inset) varies between 0.46 (CA) and 0.22 (4-HBA). For comparison, the ratio of total photon flux in the 300–400 nm range at 60° SZA to that of 0° SZA is approximately 0.5 (Fig. S1). For CA, scaling lifetime based on total flux in the 300–400 nm range may be a suitable approximation, but this will result in greater error, 30% or more, for species whose loss is more strongly driven by solar radiation below 340 nm (*i.e.* all other

Table 2 Fitting parameters for fits to j_{eff} [SZA; 10 μM] under strongly acidic conditions for all six PhC according to eqn (5)

PhC	j_{max} [10 μM] (min^{-1})	β [10 μM] (min^{-1})	SZA_C (°)	ω (°)
CA	0.26	0.31	63.2	17.6
SYR	0.11	0.12	56.4	16.8
iVAN	0.05	0.060	55.7	16.6
VAN	0.04	0.043	55.4	16.5
DMBA	0.018	0.020	50.1	15.8
HBA	0.0036	0.0039	45.6	14.7

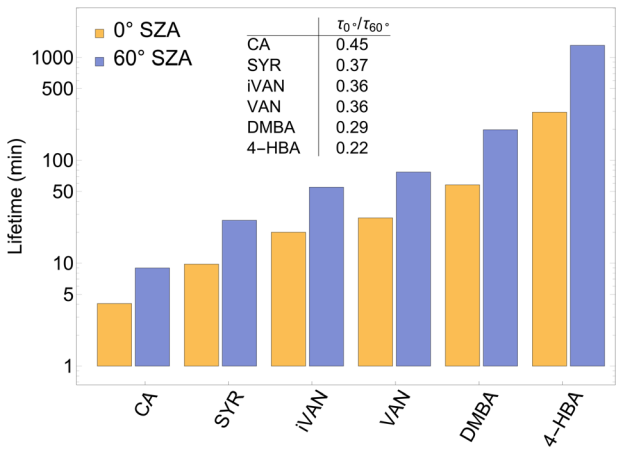

Fig. 7 Lifetime comparison between 0° SZA (yellow; 12:00, equinox at equator) and 60° SZA (blue; 12:00, Winter Solstice at 30° N latitude) for all PhC studied as 10 μM aqueous solution with pH = 2. The table inset shows the ratio of the lifetime at 0° SZA to that at 60° SZA.

PhC studied), whether due primarily to Φ_{loss} (λ), ε (λ), or their combined effects.

Utilizing Φ_{loss} (λ) to derive the SZA dependence of PhC lifetimes gives further insight into variation of photochemical loss with season and location. Assessing the hourly photochemical lifetime at a given latitude on the four limiting days of solar intensity, the equinoxes and solstices, allows an estimate of how long a given molecule will remain in an atmospheric aqueous phase. For molecules with rapid photochemical loss, we can conservatively estimate that the molecule will be significantly depleted within one hour of when the lifetime reaches a value of one hour. Note that in this work we are assessing photochemical loss of PhC in acidic, aqueous aerosol without accounting for ionic strength or other organic content. Results for CA, VAN, and 4-HBA in a range of latitudes (equatorial to 52°) for the equinoxes and solstices are shown in Fig. S6. Following this approach, CA is seen to rarely persist in sunlight for periods of more than 1–2 hours, and in the midday sun it will have an atmospheric lifetime of much less than an hour. VAN can generally persist for 3–4 hours in morning sun, but will last less than ~1–2 h in midday sun, except near the winter solstice above ~30° latitude, giving a photochemical lifetime of closer to ~1–2 days. The least substituted PhC, 4-HBA, can persist in the atmospheric aqueous phase for multiple days, even near the equinox at the equator, because its minimum lifetime is ~17 h. At higher latitudes near the winter solstice, 4-HBA can reach photochemical lifetimes of more than 2 weeks, longer than the lifetime of a typical tropospheric aerosol.

3.6 Cross reactions of PhC: insight into reactivity

To better understand the complex photodegradation characteristics of PhC molecules in aerosols, experiments were performed with solutions containing a pair of PhC molecules, one of which was CA. CA was chosen as a common reaction partner because it is the only PhC studied with significant absorption at 370 nm. CA can thus be selectively excited, so that the only excited triplet species generated is ^{3}CA*. VAN and SYR were chosen as reaction partners to demonstrate the effect of substitution on the relative ability for H-atom donation. Furthermore, the concentrations of VAN and SYR were five to ten times higher than CA to promote reaction between ^{3}CA* and non-CA H-atom donors. Results for the cross-reaction experiments are shown in Fig. 8. In the mixture of 10 μM CA with 50 μM VAN, a loss of CA occurred along with formation of CA dimers, but no loss of VAN was observed. Furthermore, Φ_{loss} for CA was essentially unchanged within measurement uncertainty (0.06). Increasing the VAN concentration to 100 μM had no discernible effect on product formation or Φ_{loss} for CA. For the 10 μM CA and 50 μM SYR mixture, CA showed significant loss while SYR was only depleted by 5%. These results indicate greater reactivity for ^{3}CA* with SYR compared to VAN, likely *via* H-atom donation, although the predominant reaction was apparently still ^{3}CA* + CA. Interestingly, dimers of CA were formed, but a stable cross-reaction dimer composed of the monomers of CA and SYR was not formed. Further investigation is warranted to clarify the origins of the selective reactivity within mixtures of PhC.

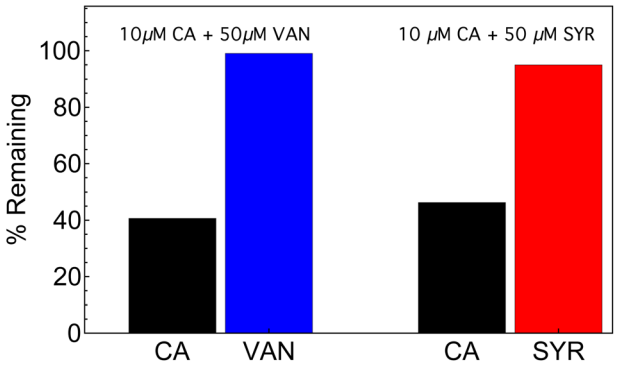

Fig. 8 The % remaining in mixed PhC irradiation experiments, using excitation at 370 nm to only produce ^{3}CA*. Despite a higher concentration of VAN and SYR (50 μM) compared to CA (50 μM) only CA is lost in significant amounts, with only 5% loss of SYR and essentially no loss of VAN.

4 Conclusions

Photochemical reactions of phenolic carbonyls (PhC) in acidic, aqueous solution depend strongly on molecular structure, excitation wavelength, and concentration. Wavelength-dependent measurements of the quantum yield for loss, Φ_{loss} (λ), along with molar absorptivity and solar radiation models, allow direct calculation of the rate of photochemical loss of PhC. The wavelength dependence of Φ_{loss} (λ) varies significantly across PhC structures. Additional conjugation, as in cinnamic acid derivatives such as CA, leads to Φ_{loss} (λ) with a peaked profile, while non-conjugated PhC show profiles with roughly exponential decay. All PhC were determined to have fast photochemical loss; methoxy substituted PhC have lifetimes of less than 1–2 h even during mid-day on the winter solstice near 30° latitude. Our results suggest extrapolations of SZA dependence from a single polychromatic light source may underestimate photochemical losses, potentially by more than a factor of 2 in the case of PhC. This may be attributed, at least in part, to the importance of the SZA dependence for 300–340 nm solar radiation. The SZA dependence of all PhC studied is similar, spanning a relatively narrow range in the scope of atmospheric photochemical reactions. Photochemical loss of PhC in aqueous, acidic solution has SZA dependence similar to that of ~315 nm solar radiation, which is similar to the SZA dependence for photolysis of aqueous nitrate ion.

Investigation into the mechanism of photochemical loss of several PhC has revealed a number of key molecular insights about their reactivity. The electronic transitions from photon absorption in the 300–400 nm range for all substituted PhC are $\pi \rightarrow \pi^*$, while the simplest PhC, 4-HBA, has a very weak $n \rightarrow \pi^*$ transition that does not result in efficient loss. When describing excited states in the NTO framework of electron–hole pairs, the character of the orbitals with increased electron density is consistent across molecular structures. In other words, the π^* character of the $\pi \rightarrow \pi^*$ transition for 300–400 nm PhC transitions is conserved. While all PhC studied have two transitions, substituent symmetry, as in the case of

SYR and DMBA, can lead to nearly degenerate $\pi \rightarrow \pi^*$ transitions that appear as a single peak in the UV spectrum. For substituted PhC, the lowest energy transition, S_1, is a dark $n \rightarrow \pi^*$ state, except for CA. The S_1 state for CA is $\pi \rightarrow \pi^*$, and its increased conjugation lowers its energy below that of the dark S_2 state involved in its $n \rightarrow \pi^*$ transition. The availability for H-atom abstraction at the position *para* to the phenol group leads to more efficient loss and products that absorb much more strongly at wavelengths >340 nm. PhC that are substituted at both the *ortho* and the *para* position relative to the phenol group (*e.g.* SYR and DMBA) and unsubstitued PhC (*e.g.* 4-HBA) do not appear to form dimer products. Increased conjugation, as in the case of CA, does not necessarily lead to strongly absorbing products, likely due to stabilized resonance structures of radical species that yield less conjugated dimer species.

The results presented highlight key considerations for assessing BrC photochemistry in atmospheric systems affected by wildfire emissions. Considering location and season, photoreactive BrC may have lifetimes with a very wide range, from the lifetime of a tropospheric aerosol down to minutes. We have shown the importance of substitution patterns on photochemistry, which may be correlated to reactivity in complex mixtures. Combined with improved characterization from advances in chromatographic methods with mass spectrometric detection, these results suggest a path toward defining wildfire photochemical reactivity by classes or features of molecules without speciation of all chromophores.[54] Our new results on cross-reactions between PhC and the role of H-atom transfer in triplet state excited species further suggests the need for studies involving more complex aerosol composition, but in a targeted manner. Cross reactions of excited state PhC species show complex, unexpected reactivity; this may extend to the host of other highly oxidized species in wildfire aerosols (*e.g.* sugars). Previous work involving UV irradiation of particulate smoke has shown whole smoke to have much longer lifetimes, in terms of absorbance, than individual BrC compounds identified in the same smoke.[23] This suggests the need to further refine identification of photochemically reactive structures and/or the effects of aerosol composition on the rates of photochemical loss or production of new absorbing species. As shown in Fig. 3, alternate H-atom donors can slow photochemical loss of organic triplet states if the resulting $PhC^{\bullet}_{+H}$ reacts with O_2 to regenerate ground state PhC, as has been used in superoxide generation schemes.[65] Finally, recent modeling of BrC suggests categorization into sub-categories of inert-, reactive-, and photobleached-BrC.[66] Developing relationships between common BrC molecular classes (*e.g.* PAH, aromatic carbonyls, nitro compounds), their wavelength dependent photochemistry, and their products post-irradiation may be a promising route to link broad chemical categorization of aerosol and modeling BrC globally.

Author contributions

Conceptualization: GTD. Formal analysis: GTD, DL, EM, YH, TW, AZ, MG, LRM. Funding acquisition: GTD. Investigation: GTD, DL, EM, YH, TW, AZ, AG, MG, LRM. Methodology: GTD, DL, EM, YH. Computational methodologies: MG, LRM. Project administration: GTD. Visualization: GTD, DL, EM, MG, LRM. Writing – first draft: DL, EM, LRM, GTD. Writing – review & editing: DL, EM, GTD, LRM.

Conflicts of interest

There are no conflicts to declare.

Data availability

Data for this article, including the figures in the main text and supplementary information (SI), are available on Zenodo at **https://doi.org/10.5281/zenodo.15803112**. Supplementary information: a data table and interpolations of wavelength dependent quantum yields, optimized geometries for molecular structure and computational spectra, fits to solar zenith angle dependence, analysis of seasonal photochemical loss rates, solar spectrum analysis, molecular structure images, computational spectra. See DOI: **https://doi.org/10.1039/d5ea00077g**.

Acknowledgements

This work was funded by the Buck Lab for Environmental Science. We acknowledge the support of Colby College and the Advanced Research Computing team and the National Science Foundation (grant no. CC*: 1659142) for supporting the Natural Science Computing Cluster, which provided the computing resources used in this work. The authors thank J. Katz for many helpful discussions on radical structure and reactivity.

Notes and references

1 J. J. Schauer, M. J. Kleeman, G. R. Cass and B. R. T. Simoneit, *Environ. Sci. Technol.*, 2001, **35**, 1716–1728.
2 C. D. Simpson, M. Paulsen, R. L. Dills, L. J. Liu and D. A. Kalman, *Environ. Sci. Technol.*, 2005, **39**, 631–637.
3 A. Akherati, Y. He, M. M. Coggon, A. R. Koss, A. L. Hodshire, K. Sekimoto, C. Warneke, J. D. Gouw, L. Yee, J. H. Seinfeld, T. B. Onasch, S. C. Herndon, W. B. Knighton, C. D. Cappa, M. J. Kleeman, C. Y. Lim, J. H. Kroll, J. R. Pierce and S. H. Jathar, *Environ. Sci. Technol.*, 2020, **54**, 8568–8579.
4 Y. L. Sun, Q. Zhang, C. Anastasio and J. Sun, *Atmos. Chem. Phys.*, 2010, **10**, 4809–4822.
5 A. Laskin, J. Laskin and S. A. Nizkorodov, *Chem. Rev.*, 2015, **115**, 4335–4382.
6 L. Yu, J. Smith, A. Laskin, K. M. George, C. Anastasio, J. Laskin, A. M. Dillner and Q. Zhang, *Atmos. Chem. Phys.*, 2016, **16**, 4511–4527.
7 D. Vione, A. Albinet, F. Barsotti, M. Mekic, B. Jiang, C. Minero, M. Brigante and S. Gligorovski, *Atmos. Environ.*, 2019, **206**, 197–207.
8 L. Ma, C. Guzman, C. Niedek, T. Tran, Q. Zhang and C. Anastasio, *Environ. Sci. Technol.*, 2021, **55**, 5772–5781.

9 W. Jiang, M. V. Misovich, A. P. Hettiyadura, A. Laskin, A. S. McFall, C. Anastasio and Q. Zhang, *Environ. Sci. Technol.*, 2021, **55**, 5199–5211.
10 T. Felber, T. Schaefer, L. He and H. Herrmann, *J. Phys. Chem. A*, 2021, **125**, 5078–5095.
11 M. Sun, C. K. Glenn, O. E. Hajj, K. V. Kumar, A. Anosike, R. Penland, M. A. Callaham, E. L. Loudermilk, J. J. O'Brien, R. Saleh and G. D. Smith, *ACS ES&T Air*, 2024, **1**, 989–999.
12 F. Li, S. Zhou, J. Zhao, J. Hang, H. Lu, X. Li, M. Gao, Y. Li and X. Wang, *ACS Earth Space Chem.*, 2024, **8**, 1193–1203.
13 E. G. Schnitzler, N. G. A. Gerrebos, T. S. Carter, Y. Huang, C. L. Heald, A. K. Bertram and J. P. D. Abbatt, *Proc. Natl. Acad. Sci.*, 2023, **19**, 2205610119.
14 E. A. Petersen-Sonn, M. Brigante, L. Deguillaume, J. L. Jaffrezo and C. George, *ACS Earth Space Chem.*, 2025, **9**, 533–544.
15 C. Anastasio, B. C. Faust and C. J. Rao, *Environ. Sci. Technol.*, 1997, **31**, 218–232.
16 C. George, M. Ammann, B. D'Anna, D. J. Donaldson and S. A. Nizkorodov, *Chem. Rev.*, 2015, **115**, 4218–4258.
17 Ó. Guzmán-Méndez, M. M. Reza, B. Meza, J. Jara-Cortés and J. Peón, *J. Phys. Chem. B*, 2023, **127**, 5655–5667.
18 S. Rossignol, K. Z. Aregahegn, L. Tinel, L. Fine, B. Nozière and C. George, *Environ. Sci. Technol.*, 2014, **48**, 3218–3227.
19 R. J. Weber, H. Guo, A. G. Russell and A. Nenes, *Nat. Geosci.*, 2016, **9**, 282–285.
20 A. Zhang, Y. Zeng, X. Yang, J. Zhai, Y. Wang, C. Xing, B. Cai, S. Shi, Y. Zhang, Z. Shen, T. M. Fu, L. Zhu, H. Shen, J. Ye and C. Wang, *Geophys. Res. Lett.*, 2023, **50**, e2023GL106541.
21 Y. Chen and T. C. Bond, *Atmos. Chem. Phys.*, 2010, **10**, 1773–1787.
22 C. E. Stockwell, P. R. Veres, J. Williams and R. J. Yokelson, *Atmos. Chem. Phys.*, 2015, **15**, 845–865.
23 L. T. Fleming, P. Lin, J. M. Roberts, V. Selimovic, R. Yokelson, J. Laskin, A. Laskin and S. A. Nizkorodov, *Atmos. Chem. Phys.*, 2020, **20**, 1105–1129.
24 W. Li, P. Ge, M. Chen, J. Tang, M. Cao, Y. Cui, K. Hu and D. Nie, Tracers from biomass burning emissions and identification of biomass burning, *Atmosphere*, 2021, **12**, 1401–1420.
25 Y. Liang, C. N. Jen, R. J. Weber, P. K. Misztal and A. H. Goldstein, *Atmos. Chem. Phys.*, 2021, **21**, 5719–5737.
26 K. Siemens, T. Paik, A. Li, F. Rivera-Adorno, J. Tomlin, Q. Xie, R. K. Chakrabarty and A. Laskin, *ACS Earth Space Chem.*, 2024, 1416–1428.
27 B. R. G. Mabato, Y. J. Li, D. D. Huang and C. K. Chan, *Environ. Sci. Technol.*, 2024, **58**, 7924–7936.
28 J. D. Smith, H. Kinney and C. Anastasio, *Atmos. Environ.*, 2016, **126**, 36–44.
29 G. T. Drozd, T. Weltzin, S. Skiffington, D. Lee, R. Valiev, T. Kurtén, L. R. Madison, Y. He and L. Gargano, *Environ. Sci.: Atmos.*, 2024, **4**, 509–518.
30 R. R. Valiev, Y. He, T. Weltzin, A. Zhu, D. Lee, E. Moore, A. Gee, G. Drozd and T. Kurten, *Phys. Chem. Chem. Phys.*, 2025, **27**, 998–1007.
31 E. S. Galbavy, K. Ram and C. Anastasio, *J. Photochem. Photobiol., A*, 2010, **209**, 186–192.
32 E. Stadler, A. Eibel, D. Fast, H. Freißmuth, C. Holly, M. Wiech, N. Moszner and G. Gescheidt, *Photochem. Photobiol. Sci.*, 2018, **17**, 660–669.
33 K. J. Angle, D. R. Crocker, R. M. C. Simpson, K. J. Mayer, L. A. Garofalo, A. N. Moore, S. L. M. Garcia, V. W. Or, S. Srinivasan, M. Farhan, J. S. Sauer, C. Lee, M. A. Pothier, D. K. Farmer, T. R. Martz, T. H. Bertram, C. D. Cappa, K. A. Prather and V. H. Grassian, *Proc. Natl. Acad. Sci.*, 2021, **118**, 2018397118.
34 G. Zheng, H. Su, S. Wang, M. O. Andreae, U. Pöschl and Y. Cheng, *Science*, 2020, **369**, 1374–1377.
35 H. O. Pye, A. Nenes, B. Alexander, A. P. Ault, M. C. Barth, S. L. Clegg, J. L. Collett, K. M. Fahey, C. J. Hennigan, H. Herrmann, M. Kanakidou, J. T. Kelly, I. T. Ku, V. F. McNeill, N. Riemer, T. Schaefer, G. Shi, A. Tilgner, J. T. Walker, T. Wang, R. Weber, J. Xing, R. A. Zaveri and A. Zuend, *Atmos. Chem. Phys.*, 2020, **20**, 4809–4888.
36 T. A. Gawargy, B. Wang and J. C. Scaiano, *Photochem. Photobiol.*, 2022, **98**, 429–433.
37 M. J. Frisch, G. W. Trucks, H. B. Schlegel, G. E. Scuseria, M. A. Robb, J. R. Cheeseman, G. Scalmani, V. Barone, G. A. Petersson, H. Nakatsuji, X. Li, M. Caricato, A. V. Marenich, J. Bloino, B. G. Janesko, R. Gomperts, B. Mennucci, H. P. Hratchian, J. V. Ortiz, A. F. Izmaylov, J. L. Sonnenberg, D. Williams-Young, F. Ding, F. Lipparini, F. Egidi, J. Goings, B. Peng, A. Petrone, T. Henderson, D. Ranasinghe, V. G. Zakrzewski, J. Gao, N. Rega, G. Zheng, W. Liang, M. Hada, M. Ehara, K. Toyota, R. Fukuda, J. Hasegawa, M. Ishida, T. Nakajima, Y. Honda, O. Kitao, H. Nakai, T. Vreven, K. Throssell, J. A. Montgomery Jr, J. E. Peralta, F. Ogliaro, M. J. Bearpark, J. J. Heyd, E. N. Brothers, K. N. Kudin, V. N. Staroverov, T. A. Keith, R. Kobayashi, J. Normand, K. Raghavachari, A. P. Rendell, J. C. Burant, S. S. Iyengar, J. Tomasi, M. Cossi, J. M. Millam, M. Klene, C. Adamo, R. Cammi, J. W. Ochterski, R. L. Martin, K. Morokuma, O. Farkas, J. B. Foresman and D. J. Fox, *Gaussian 16*, Gaussian Inc, Wallingford CT, 2016.
38 A. D. Becke, *J. Chem. Phys.*, 1993, **98**, 5648–5652.
39 P. J. Stephens, F. J. Devlin, C. F. Chabalowski and M. J. Frisch, *J. Phys. Chem.*, 1994, **98**, 11623–11627.
40 C. Lee, W. Yang and R. G. Parr, *Phys. Rev. B: Condens. Matter Mater. Phys.*, 1988, **37**, 785–789.
41 S. Vosko, L. Wilk and M. Nusair, *Can. J. Phys.*, 1980, **59**, 1200–1211.
42 T. Clark, J. Chandrasekhar, G. W. Spitznagel and P. V. R. Schleyer, *J. Comput. Chem.*, 1983, **4**, 294–301.
43 R. Krishnan, J. S. Binkley, R. Seeger and J. A. Pople, *J. Chem. Phys.*, 1980, **72**, 650–654.
44 M. Cossi, N. Rega, G. Scalmani and V. Barone, *J. Comput. Chem.*, 2003, **24**, 669–681.
45 R. L. Martin, *J. Chem. Phys.*, 2003, **118**, 4775–4777.
46 R. Dennington, T. A. Keith and J. M. Millam, *GaussView Version 6*, Semichem Inc., Shawnee Mission KS, 2019.
47 G. Loisel, M. Mekic, S. Liu, W. Song, B. Jiang, Y. Wang, H. Deng and S. Gligorovski, *Atmos. Environ.*, 2021, **246**, 118140.

48 F. Li, S. Zhou, L. Du, J. Zhao, J. Hang and X. Wang, *Sci. Total Environ.*, 2023, **856**, 158895.
49 C. G. Nolte, J. J. Schauer, G. R. Cass and B. R. Simoneit, *Environ. Sci. Technol.*, 2001, **35**, 1912–1919.
50 O. V. Vusovich, I. N. Lapin, V. A. Svetlichnyi, N. B. Sul'timova and O. N. Tchaikovskaya, *Russ. Phys. J.*, 2014, **56**, 72–75.
51 Y. Wang, M. Mekic, P. Li, H. Deng, S. Liu, B. Jiang, B. Jin, D. Vione and S. Gligorovski, *Environ. Sci. Technol.*, 2021, **55**, 4553–4564.
52 B. R. G. Mabato, Y. Lyu, Y. Ji, Y. J. Li, D. D. Huang, X. Li, T. Nah, C. H. Lam and C. K. Chan, *Atmos. Chem. Phys.*, 2022, **22**, 273–293.
53 Y. Wang, W. Huang, L. Tian, Y. Wang, F. Li, D. D. Huang, R. Zhang, B. R. G. Mabato, R. J. Huang, Q. Chen, X. Ge, L. Du, Y. G. Ma, M. Gen, K. I. Hoi, K. M. Mok, J. Z. Yu, C. K. Chan, X. Li and Y. J. Li, *ACS Earth Space Chem.*, 2022, **6**, 1115–1125.
54 A. Laskin, C. P. West and A. P. Hettiyadura, *Chem. Soc. Rev.*, 2025, **54**, 1583–1612.
55 C. Li, Q. He, A. P. S. Hettiyadura, U. Käfer, G. Shmul, D. Meidan, R. Zimmermann, S. S. Brown, C. George, A. Laskin and Y. Rudich, *Environ. Sci. Technol.*, 2020, **54**, 1395–1405.
56 A. Lavi, P. Lin, B. Bhaduri, R. Carmieli, A. Laskin and Y. Rudich, *ACS Earth Space Chem.*, 2017, **1**, 637–646.
57 H. A. Al-Abadleh, M. S. Rana, W. Mohammed and M. I. Guzman, *Environ. Sci. Technol.*, 2021, **55**, 209–219.
58 H. Chin, K. S. Hopstock, L. T. Fleming, S. A. Nizkorodov and H. A. Al-Abadleh, *Environ. Sci.: Atmos.*, 2021, **1**, 64–78.
59 N. Singh, P. J. O'Malley and P. L. Popelier, *Phys. Chem. Chem. Phys.*, 2005, **7**, 614–619.
60 G. T. Drozd, K. S.-M. Brown and H. Q. Karp, *ACS Earth Space Chem.*, 2022, **6**, 1772–1781.
61 F. A. Rivera-Adorno, L. Azzarello, M. A. Robinson, Z. C. Decker, R. A. Washenfelder, K. Hayden, A. Franchin, C. D. Holmes, C. J. Young, C. D. Fredrickson, B. Palm, C. Schmidt, A. Soja, E. Gargulinski, S. S. Brown, A. M. Middlebrook and A. Laskin, *ACS Earth Space Chem.*, 2025, **9**, 64–75.
62 H. Lignell, M. L. Hinks and S. A. Nizkorodov, *Proc. Natl. Acad. Sci. U. S. A.*, 2014, **111**, 13780–13785.
63 A. B. Dalton and S. A. Nizkorodov, *Environ. Sci. Technol.*, 2021, **55**, 14586–14594.
64 A. B. Dalton, S. M. Le, N. V. Karimova, R. B. Gerber and S. A. Nizkorodov, *Environ. Sci.: Atmos.*, 2023, **3**, 257–267.
65 M. McDowell, A. Bakac and J. Espenson, *Biochem. Biophys. Res. Commun.*, 1983, **22**, 847–848.
66 K. Skyllakou, M.-B. Korras-Carraca, C. Matsoukas, N. Hatzianastassiou, S. N. Pandis and A. Nenes, *ACS ES&T Air*, 2024, **1**, 897–908.